Human Head and Hand Effects on Semicircular PIFA Antenna and SAR Analysis

Malik Jasim. Hussein[1,3], Wa'il A. Godaymi Al-Tumah[2] and Ahmad H. AL-Shaheen[2]
[1]*Department of Physics, College of Science, University of Basrah, 61004 Basrah, Iraq*
[2]*Department of Physics, College of Science, University of Misan, 62001 Misan, Iraq*
[3]*General Directorate of Education in Muthanna, Ministry of Education, 66001 Muthanna, Iraq*
pgs.malik.jasim@uobasrah.edu.iq, wail.godaymi@uobasrah.edu.iq, prof.dr.ahmad@uomisan.edu.iq

Keyword: Specific Absorption Rate (SAR), Planar Inverted-F Antenna (PIFA), Biological Effects, Mobile Phone.

Abstract: A semi-circular Planar Inverted-F Antenna (PIFA) was designed for 5.8 GHz operation to support handheld wireless communication. In free space, it achieved 49.9 Ω input resistance, VSWR = 1.005, 17.38% fractional bandwidth, 4.13 dB peak gain, and ~98% efficiency. When positioned near multilayer head and hand phantoms, tissue loading shifted the resonant frequency from 5.84 GHz to 6.52 GHz, broadened the bandwidth, and distorted the radiation pattern due to scattering and absorption. Directivity increased to 7.85 dB, while realized gain dropped from 4.13 dB to 1.9 dB, indicating reduced efficiency. At 5 mm separation, maximum SAR values for head and hand tissues were 0.3181 W/kg (fat) and 0.0776 W/kg (fat), respectively, both well below the IEEE/ICNIRP limit of 1.6 W/kg. Increasing the distance to 10 mm reduced SAR to 0.2275 W/kg (head fat) and 0.0637 W/kg (hand fat), while improving reflection coefficient (–24.4 dB), stabilizing resonance at 6.17 GHz, and enhancing gain to 2.79 dB. These results confirm that the proposed antenna maintains high efficiency, stable impedance matching, and safe electromagnetic exposure levels during proximity operation with human tissues.

1 INTRODUCTION

Over the past several decades, the accelerated evolution of information and communication technologies has profoundly transformed modern life, leading to the widespread integration of electronic systems that emit electromagnetic (EM) radiation into nearly every aspect of human activity. These systems encompass diverse applications, ranging from broadcasting and radar infrastructures to satellite communications, as well as various medical and industrial instruments spanning from microwave ovens to sophisticated imaging and diagnostic equipment [1]. Among these technologies, mobile phones have become the most prevalent personal electronic devices worldwide [2]-[4].

Their unprecedented proliferation has consequently increased human exposure to electromagnetic fields (EMFs), sparking ongoing debates and extensive research concerning their potential biological and health effects [5]. Electromagnetic radiation is naturally produced by both terrestrial and cosmic phenomena and artificially generated through numerous technological applications. Natural sources include solar and cosmic radiation, atmospheric discharges such as lightning, and the weak endogenous electromagnetic fields produced within biological organisms [6]. Artificial sources, in contrast, arise from human-made technologies including wireless communication systems, television transmitters, microwave devices, and medical diagnostic tools such as magnetic resonance imaging (MRI) scanners.

The electromagnetic spectrum is typically divided into ionizing and non-ionizing regions. Ionizing radiation, such as X-rays and gamma rays, carries sufficient photon energy to break molecular bonds and ionize atoms [7], [8]. Non-ionizing radiation, encompassing ultraviolet, infrared, radiofrequency (RF), and microwave bands, lacks the energy required for ionization but can induce localized heating effects within biological tissues due to dielectric losses [9]-[12]. Because mobile devices are routinely operated in close proximity to the human body, the radiofrequency emissions they produce have been a major focus of scientific inquiry.

According to the International Telecommunication Union (ITU), global mobile

subscriptions exceeded five billion as early as 2011 [5]. This rapid growth prompted international organizations to formulate exposure guidelines aimed at safeguarding users from potential thermal and non-thermal biological effects of RF energy [12], [13]. Numerous investigations have analyzed the interaction between antenna structures and biological tissues by employing both simplified and anatomically realistic head and hand models [14]. These studies have shown that variations in tissue geometry, electrical conductivity, and dielectric constant as well as the presence of metallic components significantly influence antenna impedance, radiation efficiency, and the spatial distribution of the Specific Absorption Rate (SAR) [15], [16]. The SAR represents the rate at which RF energy is absorbed by biological tissue per unit mass [17], [18] and is mathematically expressed as:

$$SAR = \frac{\sigma|E|^2}{\rho} = C.\frac{dT}{dt}, \quad (1)$$

where $\sigma$is electrical conductivity, ρ is tissue density, E is the RMS electric field, C is specific heat, and $dT/dt$is the rate of temperature rise [9], [18], [19]. SAR is typically reported in watts per kilogram (W/kg) for either localized or averaged tissue masses [20]. To ensure safety, major organizations including IEEE [21], ICNIRP [22], FCC, and the EU have established SAR limits, summarized in Table 1.

Table 1: Safety limits to RF exposure by mobile phones.

International Organizations	psSAR (W/Kg) for head and body	psSAR in pinna (W/Kg)
FCC [23]	1.6 (1 gram of tissue in the form of a cube)	4
ICNIRP [24]	2 (10 gram of tissue)	2
IEEE C95.1-2005 [25]	2 (10 gram of tissue in the form of a cube)	4

Despite these well-defined safety limits, the long-term biological consequences of chronic RF exposure remain an active subject of research. Short-term exposure has been associated with transient effects such as fatigue, headaches, sleep disturbances, and sensory alterations [26]-[28]. Meanwhile, longitudinal epidemiological and laboratory studies have suggested potential correlations between prolonged RF exposure and neurological disorders, carcinogenic risk, and reproductive health concerns [29]–[34]. Ocular tissues particularly the lens of the eye-are considered especially vulnerable due to their limited vascularization and restricted ability to dissipate heat. Both animal and human studies have reported cataract formation following sustained high-intensity exposure [35]–[37].

Although conventional planar inverted-F antenna (PIFA) configurations have been extensively investigated, relatively little attention has been devoted to semicircular PIFA geometries and their electromagnetic coupling with layered biological tissues at realistic operating separations. Traditional rectangular or meandered PIFAs, while functionally effective, often fail to satisfy the structural and curvature constraints imposed by contemporary portable electronics. The present study addresses this research gap by focusing on a semicircular PIFA designed to operate within the 5.8 GHz Industrial, Scientific, and Medical (ISM) band-a frequency range widely utilized in Wi-Fi and short-range wireless systems. This choice ensures both practical relevance and comparability with established antenna architectures documented in prior literature.

In this context, a novel semicircular PIFA resonant at 5.8 GHz was designed and analyzed to assess its applicability for compact wireless devices. Comprehensive numerical simulations were performed to evaluate the antenna's electromagnetic behavior and corresponding SAR distribution when positioned near multilayer, anatomically realistic head and hand phantoms. The simulations considered separation distances of 5 mm and 10 mm and incorporated validated dielectric parameters for each biological layer to ensure model fidelity. The obtained results demonstrate that the proposed antenna achieves stable impedance matching, complies with international SAR limits, and maintains efficient radiation performance through optimized antenna-to-tissue spacing. Collectively, these findings establish the semicircular PIFA as a compact, high-performance, and biologically compatible antenna configuration well suited for next-generation portable and wearable communication systems.

2 GEOMETRIES OF ANTENNA

The geometrical top view, back view and side view of the proposed patch antenna are shown in Figure 1, respectively. A semicircular antenna was designed to operate at a frequency of 5.8 GHz. The ground plane dimensions are 16 mm by 19 mm. The patch antenna is fabricated on the two layers insulating substrates, the lower one is, FR4-Epoxy substrate with thickness (h1) of 1.6 mm, relative permittivity (ε_r) of 4.4 and loss tangent (tan δ) of 0.02, and the second is air, with

a height (h2) of 2 mm. The equivalent relative dielectric constant of 1.52 was calculated using the equation [38], [39]:

$$\varepsilon_{eqr} = \frac{\varepsilon_{r1}\varepsilon_{r2}(h_1+h_2)}{\varepsilon_{r1}h_2+\varepsilon_{r2}h_1}. \quad (2)$$

Where:

- ε_{r1}, h1 are relative dielectric constant and thickness of the lower substrate layers.
- ε_{r2}, h2 are relative dielectric constant and thickness of the upper substrate layers.

The antenna radius was calculated using (1):

$$r = 0.005\left(\frac{4}{\pi}\left(\frac{c}{4f_r\sqrt{\frac{\epsilon_{r+1}}{2}}} - H\right)\right)^2 + 0.57\left(\frac{4}{\pi}\left(\frac{c}{4f_r\sqrt{\frac{\epsilon_{r+1}}{2}}} - H\right)\right) + 2.3. \quad (3)$$

Where:

- r is radius of patch;
- H is the total height of patch;
- ε_r is the equivalent relative dielectric constant;

which was found is about to 9 mm, therefore the shorting strip width is 18mm. A probe feed technique with input impedance of 50 Ω was used, feed location is (0,8mm). High Frequency Structure Simulation (HFSS) used as tool to carry out the analysis and enhance the performance of the suggested antenna.

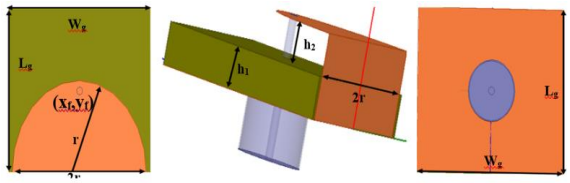

a-Top view *b- Side view* *c- Bottom view*

Figure1: proposed PIFA (a)Top view, (b) Side view and (c) Back side.

3 RESULTS AND DISCUSSION

A comprehensive assessment of the proposed semi-circular PIFA antenna has been carried out, with emphasis placed on its radiation performance, impedance characteristics, and interaction with biological media. All simulations were executed using ANSYS HFSS, a widely validated full-wave electromagnetic solver. The antenna was first analyzed under free-space conditions. As illustrated in Figure 2, the structure achieved a minimum backscatter loss of –51.91 dB at 5.84 GHz, corresponding to a fractional bandwidth of 17.38%. The input matching performance is confirmed in Figure 3, where an input impedance of 49.9 Ω which is very close to the ideal 50 Ω, indicating excellent matching performance.

These results demonstrate that the optimized design parameters, including the calculated radius and feed position, were properly selected according to the S11 criterion. The radiation characteristics were examined as illustrated in Figures 4 and 5. Figure 4 presents the 2D-radiation pattern, while Figure 5 shows the corresponding directivity distribution. A maximum directivity of 4.2dB was observed at 6GHz, and the radiation efficiency was approximately 98% in both the E- and H-planes. Figure 6 illustrates the gain performance, where the maximum gain of 4.13dB is achieved at the resonant frequency of 5.84GHz.

These findings verify the validity of the design in free space, highlighting its suitability for high-performance wireless applications.

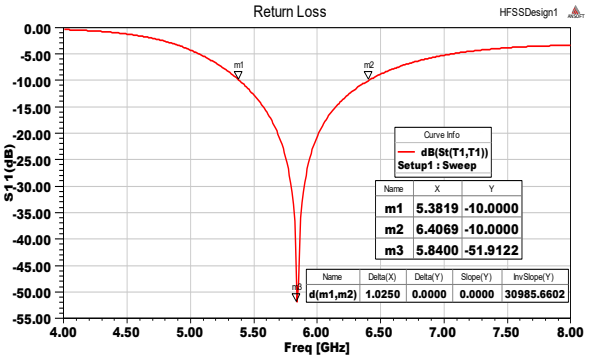

Figure 2: Return Loss for the proposed antenna in free space.

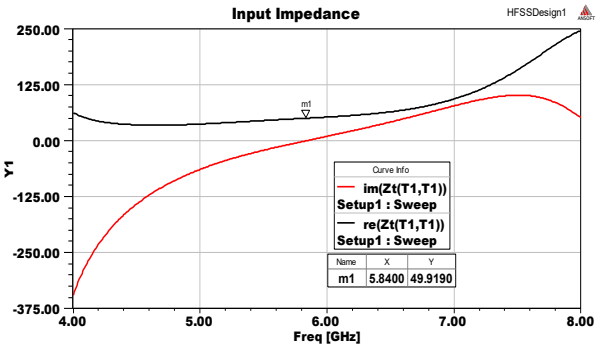

Figure 3: Input Impedance for the proposed antenna.

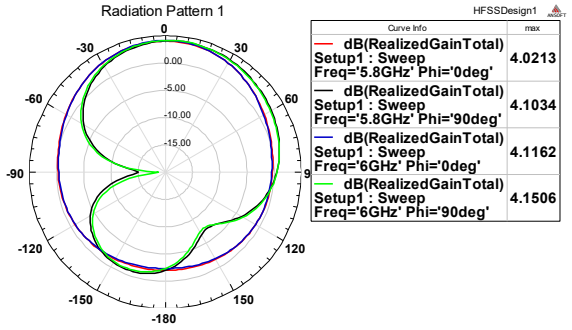

Figure 4: 2D-Total gain in dB in the principal planes for the proposed antenna.

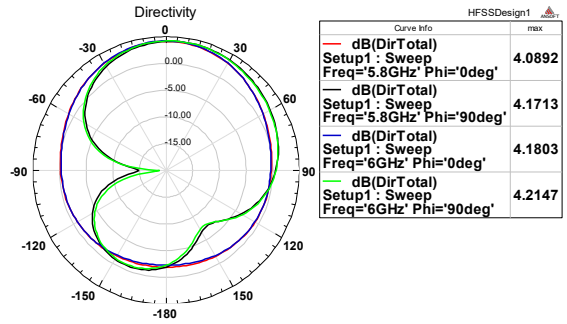

Figure 5: 2D-Total Directivity in dB in the principal planes for the proposed antenna.

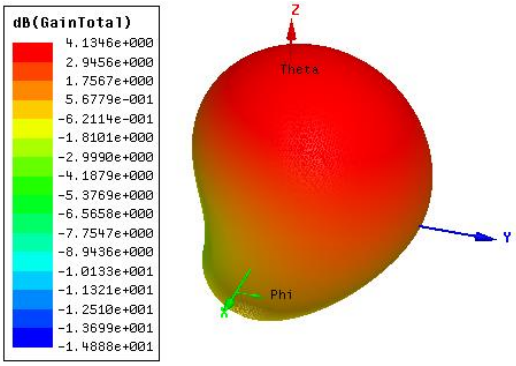

Figure 6: 3D-Total gain in dB for the proposed antenna in free space.

After finalizing the theoretical design of the semicircular Planar Inverted-F Antenna (PIFA) using HFSS simulation software, the antenna was physically built in the Antennas Laboratory at the University of Basrah as shown in Figure 7.

a-Top view b- Side view c- Bottom view

Figure 7: The prototype proposed PIFA antenna.

To validate the antenna's performance under practical conditions, experimental characterization of the reflection coefficient (S11) was conducted using a Vector Network Analyzer (PLANAR 804/1).

The resulting measurements were subsequently compared with the simulation data to assess the fidelity of the design process. As illustrated in Figure 8, the simulated response demonstrated a resonant frequency of 5.84 GHz with a minimum S11 of -51.9 dB, signifying a very high degree of impedance matching. This was corroborated by the experimental results, which recorded a minimum S11 of -36.8 dB at the identical resonant frequency, thereby confirming robust matching in the physical prototype. A comparative analysis of the impedance bandwidth further solidifies the design's accuracy.

The simulation predicted a -10 dB bandwidth spanning from 5.38 GHz to 6.40 GHz, corresponding to an absolute bandwidth of 1.02 GHz. The measured prototype exhibited a -10 dB bandwidth from 5.48 GHz to 6.30 GHz, or 0.82 GHz. This results in a stable center resonance frequency and a slight 0.20 GHz decrease in operating bandwidth. The close quantitative agreement between these datasets provides strong validation of the simulation model. The slight observed discrepancies in bandwidth depth and magnitude are consistent with typical engineering tolerances and can be reasonably attributed to factors not fully captured in the idealized simulation environment. These include minor fabrication inaccuracies, imperfections in the soldering of the feed connector, subtle variations in the dielectric constant of the substrate material, and the influence of the test environment. The overall strong correlation between the simulated and measured results not only confirms the reliability of the design methodology but also underscores the antenna's viability for practical deployment in C-band wireless systems.

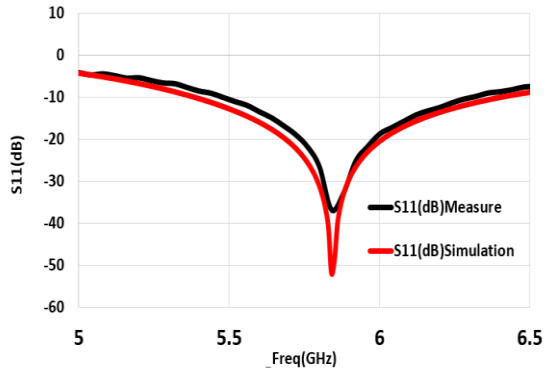

Figure 8: Simulation and measured results of proposed PIFA semicircular antenna.

Now it will be done: a comprehensive numerical model has been developed to investigate how a mobile phone antenna interacts with biological tissues of both the human head and hand, and how this interaction influences antenna performance and the SAR. The head model incorporates seven anatomically accurate layers skin, fat, bone, dura mater, cerebrospinal fluid (CSF), gray matter, and white matter arranged in their natural sequence from the outer surface inward, as illustrated in Figure 9. The dimensions of each layer are 38 mm × 32 mm and each layer was assigned specific values for thickness, relative permittivity (ε_r), and electrical conductivity (σ), based on established anatomical and electromagnetic property references [40] - [47]as shown in Table 2.

The inclusion of the dura mater and CSF layers is particularly critical, as they influence wave propagation and reflection between the skull and brain tissues, enabling realistic simulation of energy absorption within the head.

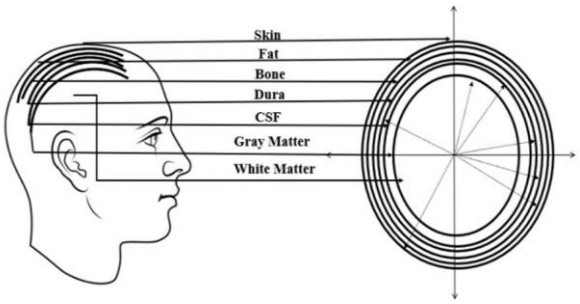

Figure 9: Seven-layered head model [40].

In typical usage scenarios, mobile phones are held close to the head and supported by the user's fingers, resulting in partial absorption of emitted electromagnetic energy by nearby tissues rather than free-space radiation. The proximity of the hand-especially the thumb to the antenna can lead to direct exposure to radio frequency (RF) radiation and alter the surrounding electromagnetic field. Previous studies have shown that the presence of the hand impacts both antenna behavior and SAR levels.

To quantify this effect, a multi-layer hand model was constructed using a methodology analogous to that of the head model. It comprises four layers: skin, fat, muscle, and bone, with each layer's thickness and electrical properties (ε_r and σ) derived from credible literature sources [45], [46], as presented in Table 3. For realistic simulation, the antenna was positioned 5 mm from the outer skin surface, as depicted in Figure 10.

Table 2: Dielectric properties of the7-head tissues at 5.84GHz.

Head Tissues	Conductivity (S/m)	Relative Permittivity	Density (kg/m³)	Tissue Thickness (mm)
Skin	3.75150	35.080	1100	1
Fat	0.29574	4.9512	920	2
Bone	1.16400	9.6564	1850	7
Dura	4.34710	37.827	1050	1.5
CSF	7.90410	60.394	1060	2
Gray Matter	5.03240	43.947	1040	3.7
White Matter	3.52640	32.580	1040	62.85

Table 3: Dielectric properties of the4-handd tissues at 5.84GHz.

Head Tissues	Conductivity(S/m)	Relative Permittivity	Density (kg/m³)	Tissue Thickness (mm)
Skin	3.75150	35.080	1100	2
Fat	0.29574	4.9512	920	2
Muscle	5.00920	48.431	1047	2
Bone	1.16400	9.6564	1850	10

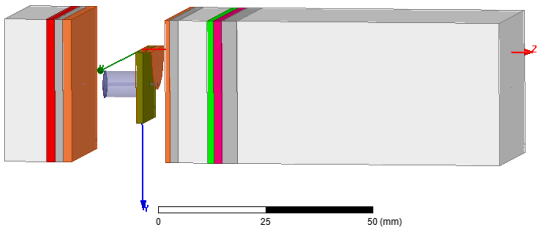

Figure 10: The simulated 7 layers head and 4 layers hand at distances 5 mm.

The antenna was analyzed in the presence of both the seven-layer head model and the four-layer hand model, providing a realistic representation of typical usage conditions, such as in handheld mobile devices. The presence of two biological media with distinct dielectric properties and conductivities introduced a more complex interaction, which strongly influenced the antenna's electromagnetic response. The most significant impact of the human head–hand model on the semicircular PIFA was frequency detuning, where the resonant frequency shifted from 5.84 GHz in free space to 6.52 GHz under combined biological loading (Fig. 11). This upward shift is attributed to the increased effective permittivity surrounding the radiator, which modifies the electromagnetic field distribution and alters the capacitive–inductive balance of the antenna. Similar behavior has been observed in recent studies on body-coupled antennas, where human tissues affect near-field reactance and dielectric loading [48]-[50].

Despite this detuning, the antenna maintained good impedance matching with a reflection coefficient of –17.09 dB, indicating that the semicircular geometry supports stable matching even under strong coupling with lossy tissues. Additionally, the operational bandwidth expanded from 5.32 GHz to 6.94 GHz, which is attributed to a reduction in the quality factor (Q) caused by absorption and scattering within the biological medium, consistent with prior observations of bandwidth broadening in high-permittivity environments [48]-[50].

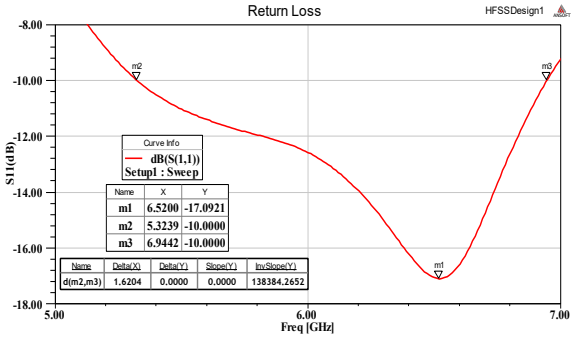

Figure 11: Simulated reflection coefficient in the presence of head and hand models at 5mm.

The radiation characteristics were more noticeably affected by the presence of biological tissues. As shown in Figure 12, the far-field pattern became distorted due to multipath scattering and reflections at tissue interfaces. Interestingly, the directivity increased to 7.85 dB at 6 GHz (Fig. 13), indicating that the human body acts as a large reflector, focusing radiated energy along specific directions. However, the realized gain decreased to 1.9 dB (Fig. 14), because a substantial portion of the directed power was absorbed by the lossy tissues, reducing the overall radiation efficiency. This physical mechanism enhanced directional concentration due to reflection combined with significant absorption-is consistent with previous analyses of antenna–human interactions [51], [52], and explains the apparent discrepancy between higher directivity and lower gain.

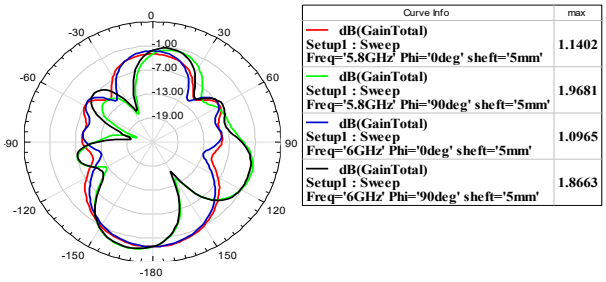

Figure 12: 2D-Total gain in dB.

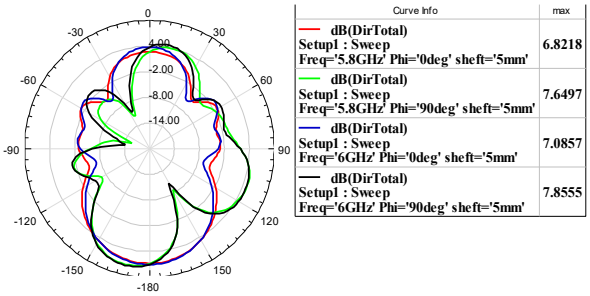

Figure 13: 2D-Total Directivity in dB.

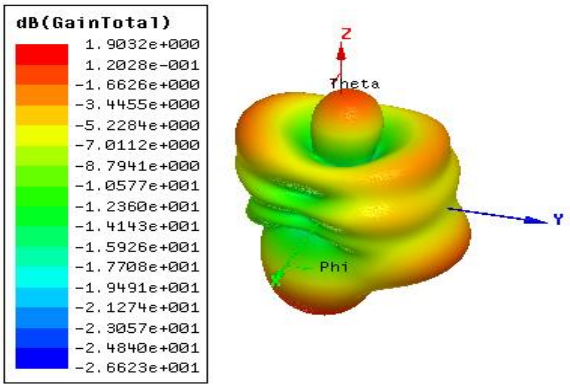

Figure 14: 3D-Total gain in dB.

The SAR was evaluated according to the 1 g averaging method, following FCC, IEEE C95.1-2005, and ICNIRP (2020) guidelines.

The SAR distributions, shown in Figures 15 and 16 at distance 5mm, revealed that energy absorption occurred across all examined layers of the head and hand. The SAR values for head tissues were: skin 0.1493 W/kg, fat 0.3181 W/kg, bone 0.1697 W/kg, dura 0.2025 W/kg, CSF 0.0972 W/kg, gray matter 0.0336 W/kg, and white matter 0.0033 W/kg. For hand tissues, the SAR values were: skin 0.0594 W/kg, fat 0.0776 W/kg, muscle 0.0276 W/kg, and bone 0.0218 W/kg. All measured SAR values remained well below the IEEE/ICNIRP safety limit of 1.6 W/kg, confirming that the proposed antenna design is safe for user operation, even in close proximity to biological tissue.

Overall, the combination of the head and hand produced the substantial frequency shift, the widest operational bandwidth, and the greatest radiation pattern distortion, accompanied by a significant reduction in gain despite an increase in directivity. These results highlight the complex electromagnetic interactions that occur when antennas are placed in close proximity to the human body, where absorption, scattering, and multipath effects jointly redefine antenna performance. Nevertheless, the SAR levels remained below internationally recognized safety limits, confirming that the proposed antenna design is suitable for practical use in modern wireless communication devices.

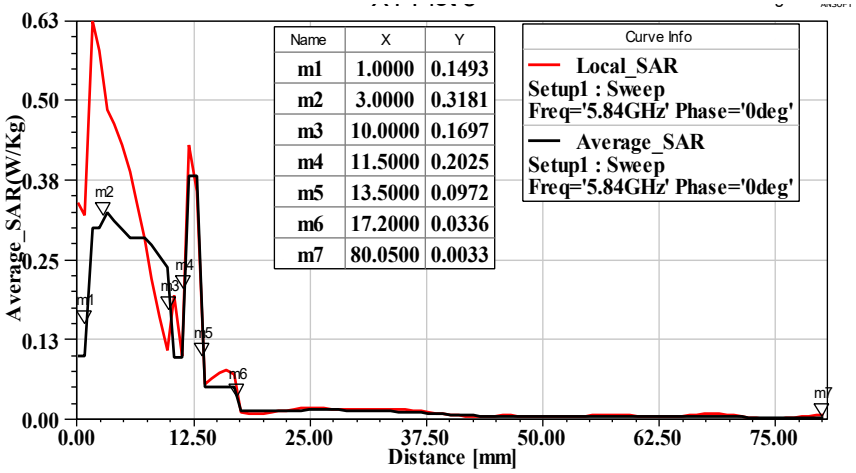

Figure 15: The SAR distribution inside the 7-layer HFSS designed head model for a PIFA antenna at 5.84 GHz at distance 5mm from the skin.

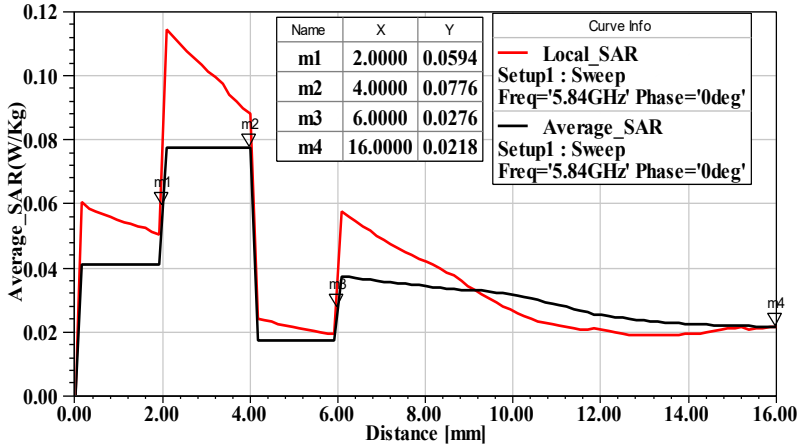

Figure 16: The SAR distribution inside the 4-layer HFSS designed hand model for a PIFA antenna at 5.84 GHz at distance 5 mm from the skin.

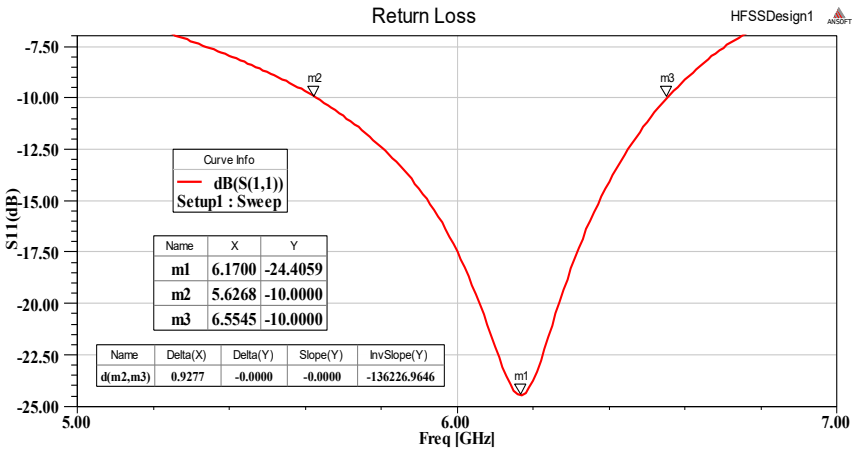

Figure 17: Simulated reflection coefficient in the presence of head and hand models at 10mm.

To investigate mitigation strategies, the antenna–tissue distance was increased from 5 mm to 10 mm. This modification reduced near-field coupling and improved several performance metrics. As depicted in Figure 17, the reflection coefficient reached –24.4 dB, with resonance shifting to 6.17 GHz and the operational bandwidth covering 5.6268–6.5545 GHz.

Radiation characteristics also improved: the two-dimensional plots (Fig. 18) indicated enhanced stability. Maximum directivity of 6.88 dB at 5.8 GHz as shows in Figure 19, while the 3D gain (Fig. 20) reached a peak of 2.79dB at resonant frequency.

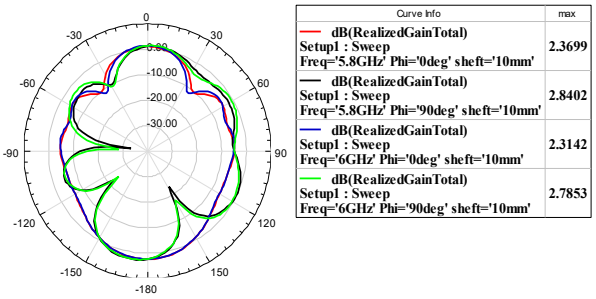

Figure 18: 2D-Total gain in dB.

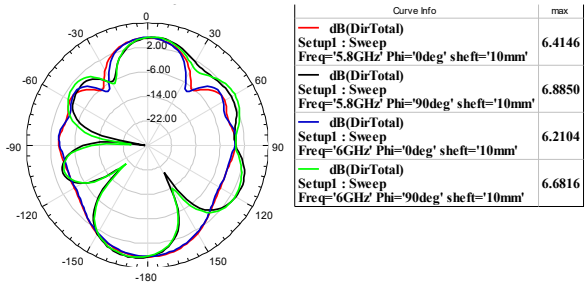

Figure 19: 2D-Total Directivity in dB.

The SAR distributions, shown in Figures 21 and 22 at distance 10mm, revealed that energy absorption occurred across all examined layers of the head and hand. The SAR values for head tissues were: skin 0.1256 W/kg, fat 0.2275 W/kg, bone 0.1324 W/kg, dura 0.1894 W/kg, CSF 0.0 887W/kg, gray matter 0.0321 W/kg, and white matter 0.0029 W/kg. For hand tissues, the SAR values were: skin 0.0477 W/kg, fat 0.0637 W/kg, muscle 0.0220 W/kg, and bone 0.0166 W/kg. All measured SAR values remained well below the IEEE/ICNIRP safety limit of 1.6 W/kg, confirming that the proposed antenna design is safe for user operation, even in close proximity to biological tissue.

Table 4 summarizes the SAR values measured for different tissues of the head and hand at two separation distances (5 mm and 10 mm) from the proposed semicircular PIFA antenna. All values are presented in W/kg and compared against the IEEE/ICNIRP safety limit of 1.6 W/kg. This comparison highlights the effect of increasing the antenna–tissue distance on reducing energy absorption.

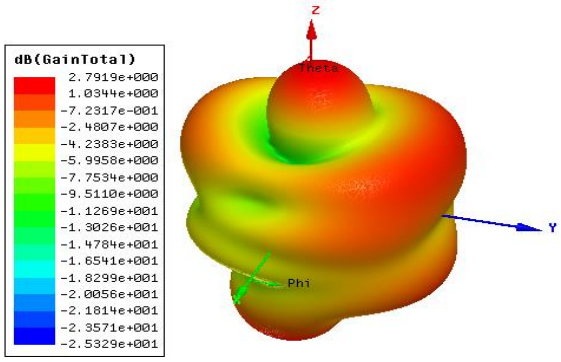

Figure 20: 3D-Total gain in dB.

As observed in Table 4, increasing the distance between the antenna and the human tissues effectively reduces SAR values, demonstrating improved safety and reduced electromagnetic interaction with the user. To evaluate the validity of the obtained results, a comparative analysis was conducted with several recent studies that reported Specific Absorption Rate (SAR) values under similar exposure conditions. Table 5 summarizes the comparison between the present work and selected recent publications (2022–2025), highlighting variations in SAR magnitude.

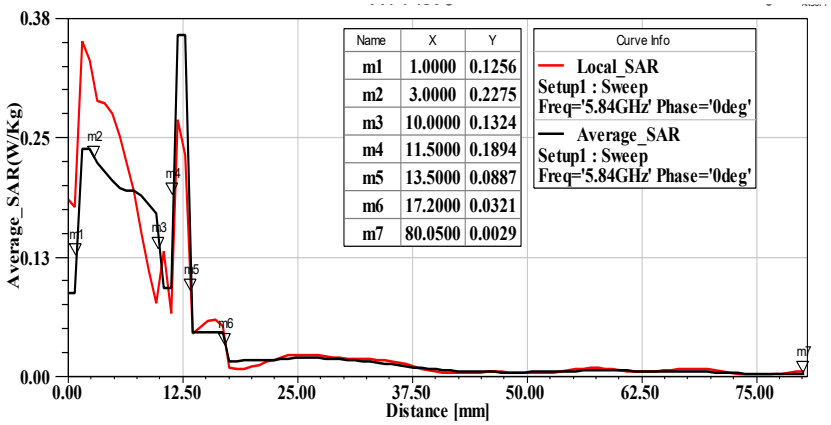

Figure 21: The SAR distribution inside the 7-layer HFSS designed head model for a PIFA antenna at 5.84 GHz at distance 10mm from the skin.

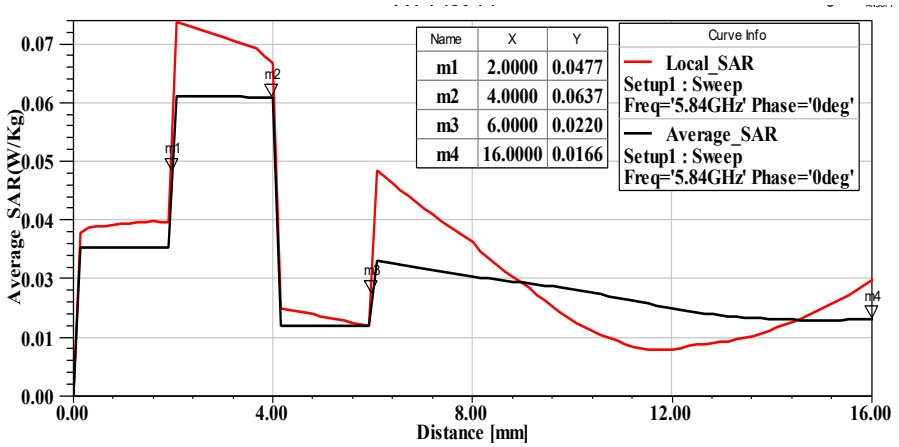

Figure 22: The SAR distribution inside the 4-layer HFSS designed hand model for a PIFA antenna at 5.84 GHz at distance 10 mm from the skin.

Table 4: SAR values for head and hand tissues at 5 mm and 10 mm (W/kg).

Head Tissues	SAR (W/kg) at 5mm	SAR (W/kg) at 10mm	Hand Tissues	SAR (W/kg) at 5mm	SAR (W/kg) at 10mm
Skin	0.1493	0.1256	Skin	0.0594	0.0477
Fat	0.3181	0.2275			
Bone	0.1697	0.1324	Fat	0.0776	0.0637
Dura	0.2025	0.1894			
CSF	0.0972	0.0887	Muscle	0.0276	0.0220
Gray Matter	0.0336	0.0321			
White Matter	0.0033	0.0029	Bone	0.0218	0.0166

Table 5: Comparison of SAR and Performance Metrics with Recent Studies.

Ref	Year	Max SAR (W/Kg)	HumanModel
[48]	2022	1.27	arm
[50]	2023	1.52	head
[51]	2024	0.89	arm
[20]	2025	1.36	head
This work	2025	0.318 at 5mm 0.247 at 10mm	Head and Hand

4 CONCLUSIONS

The proposed semicircular PIFA antenna exhibited outstanding electromagnetic performance in free space, such as wide operation bandwidth, almost ideal impedance matching, and high radiation efficiency. These results confirm the suitability of the semicircular topology for compact wireless platforms, particularly where both size constraints and multi-band operation are critical. When tested in realistic usage scenarios involving proximity to the human head and hand, the antenna exhibited notable frequency detuning, reduced realized gain, and moderate distortion in the radiation pattern. These effects are essentially related to the strong dielectric loading by biological tissues, which increases the electromagnetic absorption and changes the near-field distribution. Despite these interactions, all computed SAR values remained substantially below internationally recognized exposure limits (IEEE C95.1 and ICNIRP), highlighting the safety and compatibility of the design to be used in handheld communication devices.

However, this study is limited by the use of only one type of anatomical phantom and fixed antenna–tissue separations that may not capture all the variability in user morphology, hand placement, or head geometry. Variations in age, tissue composition, and layer thickness can lead to different detuning behaviors and absorption characteristics. Future studies may resolve these limitations by the use of multiple heterogeneous head-and-hand models, dynamic or adaptive impedance matching to reduce detuning, and the use of various SAR-reduction methods such as optimized radiator shaping, selective shielding, or the addition of absorbers. Adaptation mechanisms can be added in the form of power-

control algorithms that dynamically adjust the exposure to maintain link quality.

Overall, the semicircular PIFA antenna forms a robust and efficient solution for modern wireless devices, effectively balancing compactness with performance while meeting international safety standards. It has shown great resilience in the presence of biological loading, promising use in next-generation communication systems, which operate reliably in realistic user environments.

ACKNOWLEDGMENTS

The authors gratefully acknowledge support from the Department of Physics, College of Science, University of Basrah, Iraq.

REFERENCES

[1] R. S. Al-Mayyahi, W. A. G. Al-Tumah, and Z. A. Ahmed, "The effects of x band radar frequency exposure on mice testis and kidney," Pollut. Res., vol. 39, pp. S142–S148, 2020.

[2] J. Beekhuizen et al., "Modelling indoor electromagnetic fields (EMF) from mobile phone base stations for epidemiological studies," Environ. Int., vol. 67, pp. 22–26, 2014.

[3] B. M. Zeleke et al., "Personal exposure to radio frequency electromagnetic fields among Australian adults," Int. J. Environ. Res. Public Health, vol. 15, no. 10, p. 2234, 2018.

[4] R. S. Al-Mayyahi and A. Wa'il, "Adolescents are more sensitive than adults to the effects of radio frequency waves: A histopathological study in mice," Ecology, Environment and Conservation, vol. 27, no. 2, pp. 759–763, 2021.

[5] B. Kaur, S. Singh, and J. Kumar, "A study of SAR pattern in biological tissues due to RF exposure," in 2015 2nd International Conference on Recent Advances in Engineering & Computational Sciences (RAECS), IEEE, 2015, pp. 1–5.

[6] C. Bianchi and A. Meloni, "Natural and man-made terrestrial electromagnetic noise: an outlook," Ann. Geophys., vol. 50, no. 3, pp. 435–445, 2007.

[7] A. H. Sparrow, "Types of Ionizing Radiation and Their Cytogenetic Effects1," Publ. Acad. Sci. Res. Counc., no. 891, p. 55, 1961.

[8] E. S. Kempner, "Effects of high-energy electrons and gamma rays directly on protein molecules," J. Pharm. Sci., vol. 90, no. 10, pp. 1637–1646, 2001.

[9] J. Behari, Radio Frequency and Microwave Effects on Biological Tissues, 2019. doi: 10.1201/9780429287947.

[10] A. Zamanian and C. Hardiman, "Electromagnetic radiation and human health: A review of sources and effects," High Freq. Electron., vol. 4, no. 3, pp. 16–26, 2005.

[11] N. Khalid, M. Zubair, M. Q. Mehmood, and Y. Massoud, "Emerging paradigms in microwave imaging technology for biomedical applications: unleashing the power of artificial intelligence," npj Imaging, vol. 2, no. 1, p. 13, 2024.

[12] M. Maqbool, An Introduction to Non-Ionizing Radiation, Bentham Science Publishers, 2023.

[13] C. on N.-I. R. Protection, "ICNIRP statement on the 'Guidelines for limiting exposure to time-varying electric, magnetic, and electromagnetic fields (up to 300 GHz),'" Health Phys., vol. 97, no. 3, pp. 257–258, 2009.

[14] N. A. Samsuri, "The effect of jewellery and the human hand on SAR and antenna performance," 2009, Loughborough University.

[15] P. A. Valberg, "Radio frequency radiation (RFR): the nature of exposure and carcinogenic potential," Cancer Causes Control, vol. 8, no. 3, pp. 323–332, 1997.

[16] R. D. Morris, L. L. Morgan, and D. Davis, "Children absorb higher doses of radio frequency electromagnetic radiation from mobile phones than adults," Ieee Access, vol. 3, pp. 2379–2387, 2015.

[17] C. K. Chou et al., "Radio frequency electromagnetic exposure: Tutorial review on experimental dosimetry," Bioelectromagn. J. Bioelectromagn. Soc. Soc. Phys. Regul. Biol. Med. Eur. Bioelectromagn. Assoc., vol. 17, no. 3, pp. 195–208, 1996.

[18] V. Koncar, Smart textiles and their applications, Woodhead Publishing, 2016.

[19] L. Alon, D. K. Sodickson, and C. M. Deniz, "Heat equation inversion framework for average SAR calculation from magnetic resonance thermal imaging," Bioelectromagnetics, vol. 37, no. 7, pp. 493–503, 2016.

[20] T. Jariyanorawiss, K. Kanjanasit, W. Chongburee, and N. Sornsungnoen, "SAR Analysis in an Anatomical Head Model Using CFL-Optimized Yee Cells and an Accurate Dipole Model at 700 MHz for 5G Mobile Radiation," IEEE Access, 2025.

[21] U. S. A. IEEE, "IEEE standard for safety levels with respect to human exposure to electric, magnetic, and electromagnetic fields, 0 Hz to 300 GHz," IEEE Std C95. 1-2019 (Revision IEEE Std C95. 1-2005/Incorporates IEEE Std C95. 1-2019/Cor 1-2019), pp. 1–312, 2019.

[22] G. Ziegelberger et al., "Guidelines for limiting exposure to electromagnetic fields (100 kHz to 300 GHz)," Health Phys., vol. 118, no. 5, pp. 483–524, 2020.

[23] U.S. Code of Federal Regulations 47 CFR 2.1093, "Radiofrequency radiation exposure evaluation," 2010.

[24] "Guidelines for limiting exposure to time-varying electric, magnetic, and electromagnetic fields (up to 300 GHz). International Commission on Non-Ionizing Radiation Protection.," Health Phys., vol. 74, no. 4, pp. 494–522, Apr. 1998.

[25] 28 IEEE Standards Coordinating Committee, "IEEE standard for safety levels with respect to human exposure to radio frequency electromagnetic fields, 3kHz to 300GHz," IEEE C95. 1-1991, 1992.

[26] T. Al-Khlaiwi and S. A. Meo, "Association of mobile phone radiation with fatigue, headache, dizziness, tension and sleep disturbance in Saudi population.," Saudi Med. J., vol. 25, no. 6, pp. 732–736, 2004.

[27] M. Arns, G. Van Luijtelaar, A. Sumich, R. Hamilton, and E. Gordon, "Electroencephalographic, personality, and executive function measures associated with frequent mobile phone use," Int. J. Neurosci., vol. 117, no. 9, pp. 1341–1360, 2007.

[28] F. Kalafatakis, D. Bekiaridis-Moschou, E. Gkioka, and M. Tsolaki, "Mobile phone use for 5 minutes can cause significant memory impairment in humans.," Hell. J. Nucl. Med., vol. 20 Suppl, pp. 146–154, 2017.

[29] L. Hardell and M. Carlberg, "Mobile phones, cordless phones and the risk for brain tumours," Int J Oncol, vol. 35, no. 1, pp. 5–17, 2009, doi: 10.3892/ijo_00000307.

[30] D. Aydin et al., "Mobile phone use and brain tumors in children and adolescents: a multicenter case–control study," J. Natl. Cancer Inst., vol. 103, no. 16, pp. 1264–1276, 2011.

[31] S. Sadetzki et al., "Cellular phone use and risk of benign and malignant parotid gland tumors-a nationwide case-control study," Am. J. Epidemiol., vol. 167, no. 4, pp. 457–467, 2008.

[32] R. Czerninski, A. Zini, and H. D. Sgan-Cohen, "Risk of parotid malignant tumors in Israel (1970–2006)," Epidemiology, vol. 22, no. 1, pp. 130–131, 2011.

[33] T. N. and S. W. T. Nagaoka, "SAR Calculation in Semi-Homogeneous Human Models of Pregnancy for RF Exposure," Asia Pacific Symposium on Electromagnetic Compatibility (APEMC), pp. 444-447, 2015.

[34] T. Nagaoka, K. Saito, M. Takahashi, K. Ito, and S. Watanabe, "Anatomically realistic reference models of pregnant women for gestation ages of 13, 18, and 26 weeks," 2008. doi: 10.1109/iembs.2008.4649788.

[35] S. P. and E. P. P. Bernardi, M. Cavagnaro, "SAR Distribution and Temperature Increase in an Anatomical Model of the Human Eye Exposed to the Field Radiated by the User Antenna in a Wireless LAN," IEEE Trans. Microwave Theory Techn., vol. 46, no. 12, pp. 2074–2082, 1998.

[36] A. W. Guy, J. C. Lin, P. O. Kramar, and A. F. Emery, "Effect of 2450-MHz Radiation on the Rabbit Eye," 1975. doi: 10.1109/TMTT.1975.1128606.

[37] B. Appleton, S. E. Hirsch, and P. V. K. Brown, "Investigation of single-exposure microwave ocular effects at 3000 MHz," 1975. doi: 10.1111/j.1749-6632.1975.tb35989.x.

[38] W. L. Stutzman and G. A. Thiele, Antenna Theory and Design, Wiley, 2012.

[39] D. H. Hashim, "Design and Simulation of Arrays of Modified Circular Microstrip Antenna Excited by Two Orthogonal Feeders and Two Dielectric Substrates," University of Basrah, 2023.

[40] S. S. Pudipeddi and P. V. Y. Jayasree, "Investigation of the Effect of Normal Incidence of RF Wave on Human Head Tissues Employing Cu and Ni Grid PET Films," Eng. Technol. Appl. Sci. Res., vol. 12, no. 6, pp. 9445–9449, 2022.

[41] S. H. A. J.-Y. Chung, "Design and Characterization of a Miniaturized Implantable Antenna in a Seven-Layer Brain Phantom," IEEE Access, vol. 7, pp. 162062–162069, 2019, doi: 10.1109/ACCESS.2019.2951489.

[42] M. Särestöniemi, D. Singh, J. Reponen, M. Von und zu Fraunberg, and T. Myllylä, "Skull fracture detection for point-of-care diagnostics using microwave technique," Finnish J. eHealth eWelfare, vol. 17, no. 1, pp. 20–31, 2025, doi: 10.23996/fjhw.155481.

[43] G. A. Ahmed and A. H. Sallomi, "SAR Calculation in a Child Seven-Layer Head Model at 2.1 and 2.6 GHz," Wasit J. Comput. Math. Sci., vol. 2, no. 1, pp. 40–45, 2023.

[44] M. Alian and N. Noori, "Analysis of Multilayer Spherical Head Model Exposed to EM Radiation from Arbitrary Source Using Spherical Vector Wave Functions," Adv. Electromagn., vol. 12, no. 3, pp. 10–18, 2023, doi: 10.7716/aem.v12i3.1995.

[45] A. Sonawane and D. S. Bormane, "SAR Analysis Using a Dipole Antenna in a Non-layered and Multi-layered Human Head Model," Int. J. Recent Innov. Trends Comput. Commun., vol. 10, no. 1, pp. 225–231, 2022, doi: 10.17762/ijritcc.v10i1s.5829.

[46] H. K. and A. Cheldavi, "Irradiation of a Six-Layered Spherical Model of Human Head in the Near Field of a Half-Wave Dipole Antenna," IEEE Trans. Microwave Theory Techn., vol. 58, no. 3, Mar. 2010.

[47] "Dielectric properties of the body tissues," http://niremf.ifac.cnr.it/tissprop/htmlclie/htmlclie.php , accessed April 2020.

[48] A. Ejaz and Y. Amin, "Towards durable and efficient antenna with SAR reduction analysis for on-body applications," Frequenz, vol. 76, no. 7–8, pp. 429–439, 2022.

[49] N. H. Abd Rahman, Y. Yamada, and M. S. Amin Nordin, "Analysis on the effects of the human body on the performance of electro-textile antennas for wearable monitoring and tracking application," Materials (Basel)., vol. 12, no. 10, p. 1636, 2019.

[50] A. Z. A. Zaki et al., "Design and modeling of ultra-compact wideband implantable antenna for wireless ISM band," Bioengineering, vol. 10, no. 2, p. 216, 2023.

[51] D. Sharma, S. Kumar, R. N. Tiwari, H. C. Choi, and K. W. Kim, "On body and off body communication using a compact wideband and high gain wearable textile antenna," Sci. Rep., vol. 14, no. 1, pp. 1–17, 2024, doi: 10.1038/s41598-024-64932-6.

[52] C. Wang et al., "New advances in antenna design toward wearable devices based on nanomaterials," Biosensors, vol. 14, no. 1, p. 35, 2024.